Spatio-temporal variations of land surface temperature using Landsat and MODIS: case study of the City of Tshwane, South Africa

James Magidi [1,2] and Fethi Ahmed [2]

[1]Geomatics Department, Tshwane University of Technology, Pretoria, 0001, South Africa,
jamestmagidi@gmail.com
[2] Geography, Archaeology and Environmental Studies, University of Witwatersrand, 1 Jan Smut,
Johannesburg, South Africa

Abstract

Urbanisation is accelerating urban land use dynamics and this has a significant impact on land surface temperature (LST). Impervious surfaces and increase in air pollution has led to the increase in land surface temperature. This study reports on the use of geospatial technologies to monitor and quantify changes in LST using remotely sensed data in the City of Tshwane. Land surface temperature was retrieved using the winter and summer Landsat datasets for 1997 and 2015 and the MODIS data from 2000 to 2015. Land surface temperature was extracted using emissivity and satellite temperature as input parameters. The spatial and temporal variations in the LST were retrieved to show the effects of land cover change on LST. Change in LST was also analysed on different land cover types using transects across the study area. The study revealed an increase in land surface temperature between the years. It also showed that impervious surfaces had a higher LST compared to the non-impervious surfaces. The results revealed variations in LST between non-cropped and cropped agricultural areas, where the former had higher LST than the latter. Temporal trends revealed a notable increase in LST in the urban areas and there were some seasonal variations in LST with high LST values in summer and low values in winter. Cross-section analysis along transects revealed spatio-temporal thermal variations across different land cover types.

Keywords: Landsat, MODIS, Land Surface temperature, urban heat island, remote sensing, City of Tshwane

1. Introduction

There is an increase in global land surface temperature as a result of controlled and uncontrolled urbanisation. Urbanisation which can be defined as the increase in the number of urban dwellers is increasing at an alarming rate in both developing and developed countries leading to the transformation of non-urban environments into urban environments (Zhang, 2016). Urbanisation is one of the major global challenges which is leading to change in the properties of land surface materials (Mathew *et al.*, 2018). Urbanisation leads to urban sprawl which has an impact on the

quality of the environments, which include air quality and land surface temperature (Abutaleb *et al.*, 2014; Wray and Cheruiyot, 2015). Land Surface Temperature (LST) increases were reported in urban areas as a result of impervious surfaces and high concentration of pollutants leading to the establishment of urban heat islands (UHI) (Mallick *et al.*, 2008; Sheng *et al.*, 2017). UHI which can be defined as a microclimate where the temperature in the urban areas is higher than that of the surrounding areas (Abutaleb *et al.*, 2014; Peres *et al.*, 2018; Yue *et al.*, 2007). Urban heat Islands are a result of anthropogenic activities which influence the increase in temperature in the urban areas and these cause an increase in precipitation (Huang *et al.*, 2008; Sheng *et al.*, 2017). These UHI leads to the change in the quality of air and leads to rise in global warming (Mallick *et al.*, 2008) which can be detrimental to the human health thereby increasing mortality (Yue *et al.*, 2007).

With the rapid urbanization of the world population, research on urban microclimate has gained popularity in the past years. For sustainable management of urban areas there is a need to monitor and quantify land surface temperature in urban areas (Mushore *et al.*, 2017). Geospatial techniques such as remote sensing has been identified as very crucial, cost effective and accurate tools that are used to monitor and quantify change in the landscape parameters such as land surface temperature, urban sprawl, pollution etc. (Magidi and Ahmed, 2018; Mushore *et al.*, 2017).

Land Surface Temperature thermal profiles are used to graphically illustrate spatial variations of temperature in the urban environment and its surroundings (Sheng *et al.*, 2017). Typical thermal curves of LST variations will show cliffs, peaks, depressions and plateaus, which reveal the thermal variations (Abutaleb *et al.*, 2014; Huang *et al.*, 2008). Anthropogenic activities cause changes in the surface (from natural to impervious) which affect albedo, thermal capacity and heat conductivity (Abutaleb *et al.*, 2014). An urban area with green vegetation has lower LST than a non-vegetated urban area (Mallick *et al.*, 2008; Tomlinson *et al.*, 2012; Weng *et al.*, 2004) hence the use of vegetation indices such as the Normalised Difference Vegetation Indices (NDVI) in retrieving LST using remotely sensed data. Satellite temperature is slightly lower than the temperature measured at meteorological stations (ground level) hence the need for ground emissivity and atmospheric corrections is needed in order to accurately quantify LST (Sobrinoet *et al.*, 2004; Yin *et al.*, 2020). Vegetation cover, vigour, and soil background influence the emissivity and hence the use of NDVI in calculating emissivity (Abutaleb *et al.*, 2014; Neinavaz *et al.*, 2020; Sobrino *et al.*, 2004; Yin *et al.*, 2020).

The City of Tshwane (CoT) was also affected by urbanisation, which had led to the proliferation of planned and unplanned settlements (Magidi and Ahmed, 2018). This urban sprawl affected the microclimate in the city and the aim of this study is to assess and monitor the impact of urban sprawl on land surface temperature using remotely sensed data.

2. Study Area

City of Tshwane (CoT) as indicated on Figure 1 is situated north of the Gauteng Province, and is also the administrative capital of the Republic of South Africa (Matlala, 2015). It lies between

latitudes 25°6'34.60" S to 26°4'41.12"S and longitudes 27°53'24.26"E to 29°5'54.31" E. According to the STATSSA (2012) the city has a landmass of 629 618 ha, has a population of 2 921 490 people and 911 536 households. The CoT lies at an average elevation of 1280m above mean sea level and it falls within the grasslands biome (Mucina and Rutherford, 2006). CoT has an average temperature and rainfall of 17.8°C and 697mm respectively. The temperature and rainfall are high in summer and low winter.
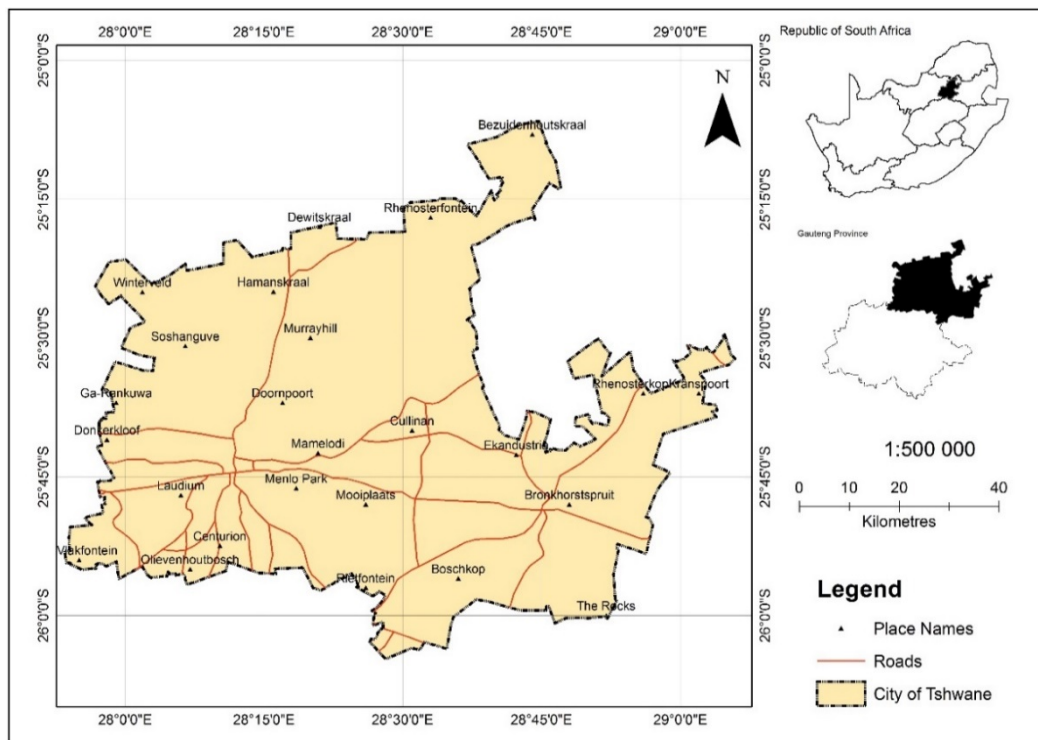

Figure 1: The study area map showing the City of Tshwane

3. Data and Methods

Remotely sensed data (Landsat OLI and Landsat TM) were downloaded from the United States Geological Surveys (USGS)'s Earth Explorer web portal. Acquired remotely sensed data for both winter and summer seasons as indicated in Table 1 were acquired from the USGS portal. Winter and summer cloud-free images were found in August (1997 and 2015) and December (1997 and 2015) respectively. Moderate Resolution Imaging Spectroradiometer (MODIS) Land Surface Temperature and Emissivity (MOD11) with a spatial resolution of 1km and 8-day temporal resolution was retrieved using Google Earth Engine for the period from 2000 to 2015. Climate data from South African Weather Services was also used in this study to augment the findings from remote sensing (Harris *et al.*, 2014). Figure 2 illustrates the flowchart of the methodology used to retrieve LST in the two years (1997 and 2015).

Table 1: Landsat TM and ETM+ remotely sensed data that was used in this study.

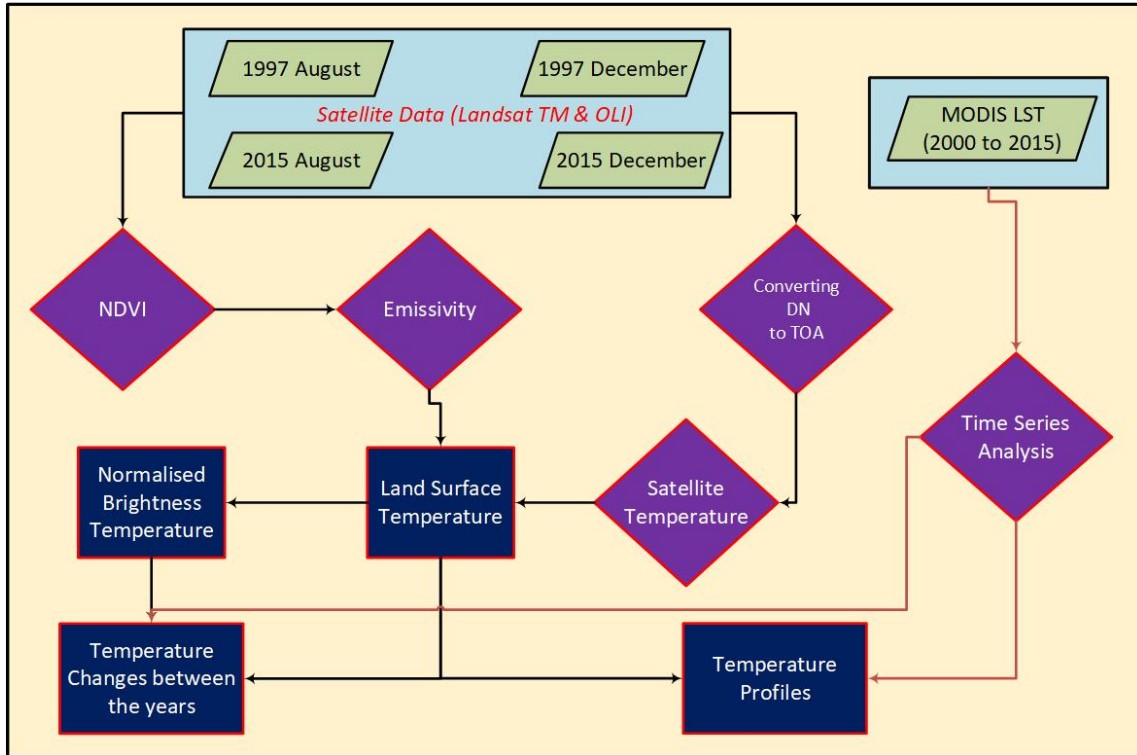| Sensor	Year	Month	Path	Row	Scene Status
Landsat OLI	2015	December			
		August	177	77 and 78	Cloud-free
Landsat TM	1997	December			
		August			

Figure 2: Flowchart showing the methods used to retrieve LST in the City of Tshwane

3.1.   Converting to Radiance

The remotely sensed data was converted from the downloaded DN (digital number) values to TOA (Top of Atmosphere Reflectance) for Landsat TM and Landsat ETM+ datasets and the formula in Equation 1 and Equation 2 were used respectively (Qin *et al.*, 2001).

$$L = (L_{\lambda max} - L_{\lambda min}) * \frac{Q_{\lambda DN} - Q_{\lambda min}}{Q_{\lambda max} - Q_{\lambda min}} + Lmin \qquad\qquad 1$$

where L= is the spectral radiance received by the sensor, $L_{\lambda max}$ is the maximum detected spectral radiance, $L_{\lambda min}$ is the minimum spectral radiance. Q_{DN} is the DN at a given pixel, $Q_{\lambda max}$ = is the maximum DN value (255) and $Q_{\lambda min}$ = is the minimum DN value (0) (Qin *et al.*, 2001)

$$L_{\lambda} = M_L Q_{cal} + A_L \qquad\qquad 2$$

where: L_{λ} = TOA spectral radiance (Watts/(m^2 * srad * μm)), M_L = Band-specific multiplicative rescaling factor from the metadata A_L = Band-specific additive rescaling factor from the metadata and Q_{cal} = Quantized and calibrated standard product pixel values (DN) (Qin *et al.*, 2001).

3.2. Calculating Satellite Temperature

Satellite temperature was retrieved from Band 6 (Landsat TM) and band 10 (Landsat OLI) using Equation 3 (Artis and Carnahan, 1982; K. S. Kumar *et al.*, 2012).

$$T_{Sat} = K_2 / \ln((K_1/L_\lambda) + 1) \qquad\qquad 3$$

where: T_{Sat} = satellite brightness temperature (K), L_λ = TOA spectral radiance (Watts/(m^2 * srad * μm)), K_1 = Band-specific thermal conversion constant (Table 2) and K_2 = Band-specific thermal conversion constant (Table 2) (Chander and Markham, 2003; K. S. Kumar *et al.*, 2012)

Table 2: Thermal Conversion Constants for Landsat

Constant	Landsat TM	Landsat ETM+	Landsat OLI
K1	607.76	666.09	In the metadata
K2	1260.56	1282.71	In the metadata

3.3. Calculating Normalised Difference Vegetation Indices (NDVI)

Normalised Difference Vegetation Indices (NDVI) is an indicator invented by Townshend and Justice (1986) and calculated from the red bands and the near-infrared bands (D. Kumar and Shekhar, 2015) as indicated in Equation 4. The NDVI formula estimates the amount of above-ground vegetation cover from red and infrared bands (D. Kumar and Shekhar, 2015). Green vegetation absorbs the red wavelengths as a result of chlorophyll while scattering near-infrared wavelengths and unhealthy leaves reflect the red band and absorb the near-infrared bands (D. Kumar and Shekhar, 2015). NDVI ranges between -1 and 1 and values between -1 and 0 where the NDVI above 0.1 is for vegetated areas (Laosuwan *et al.*, 2017).

$$NDVI = (NIR - RED)/(NIR + RED) \qquad\qquad 4$$

where: NIR is the Near Infra-Red Band (Band 4 in TM and Band 5 in OLI) and RED = Red Band (Band 3 in TM and Band 4 in OLI)

3.4. Calculating Emissivity

Emissivity is a function of wavelength, which is influenced by a number of environmental factors such as water content, chemical composition, the density of vegetation, plant species and smoothness of the surface (Sobrino *et al.*, 2004). There is a correlation between emissivity and NDVI (Nega *et al.*, 2019; Sobrino *et al.*, 2004) and conditional formulae used to compute emissivity are shown in Table 3.

Table 3: Estimation of land surface emissivity using NDVI.

NDVI	Land Surface Emissivity (ε)
NDVI<-0.185	0.995
-0.185≤NDVI≤0.157	0.970
0.157≤NDVI≤0.727	1.0094+0.047ln(NDVI)
NDVI>0.727	0.990

3.5. Calculating Land Surface Temperature (LST)

Satellite temperature (T_{Sat}) and emissivity were used to compute LST using Equation 5 (Artis and Carnahan, 1982; Chander and Markham, 2003; Weng *et al.*, 2004).

$$LST = T_{Sat}/\left(1 + [(\lambda T_{Sat}/\rho)\ln(\varepsilon)]\ \right) \qquad\qquad 5$$

where: T_{sat} is satellite temperature derived from Equation 3, λ = wavelength of emitted radiance and average wavelengths and ε is the surface emissivity derived from Table 3 (Chander and Markham, 2003).and $\rho = h(c/\sigma)$ (σ is the Stefan-Boltzmann constant ($1.38*10^{-23}$ J/K), h is the Planck's constant ($6.626*10^{-32}$Js) and *c* is the velocity of light ($2.998*10^8$ m/s).

3.6. Normalising Brightness Temperature

There is a need to normalise LST between 0 and 1 to avoid time difference when images were captured and for easy comparison of LST. Equation 6 was used to compute the normalised LST (Schissau, 2006).

$$N = (T_i - T_{min})/(T_{max} - T_{min}) \qquad\qquad 6$$

where N is the pixel normalised value of the LST, T_i is the LST of the ith pixel, T_{min} is the minimum value of the LST and T_{max} is the maximum LST. The normalised LST can be divided into five zones, which are strong heat islands zone (0.8-1.0), heat islands zone (0.6-0.8), normal zone (0.4-0.6), green islands zone (0.2-0.4) and strong green islands zone (0-0.2) (El-Magd *et al.*, 2016; Xu *et al.*, 2013).

3.7. Cross-Sectional Analysis using Transects

Transects as indicated in Figure 3 were across different land cover classes using the 3D Analyst in ArcGIS (ESRI, 2015). Transects were created across agricultural areas, across the city centres, across the residential areas and across city outskirts. The LST on each point on the transect was recorded and results were computed graphically.
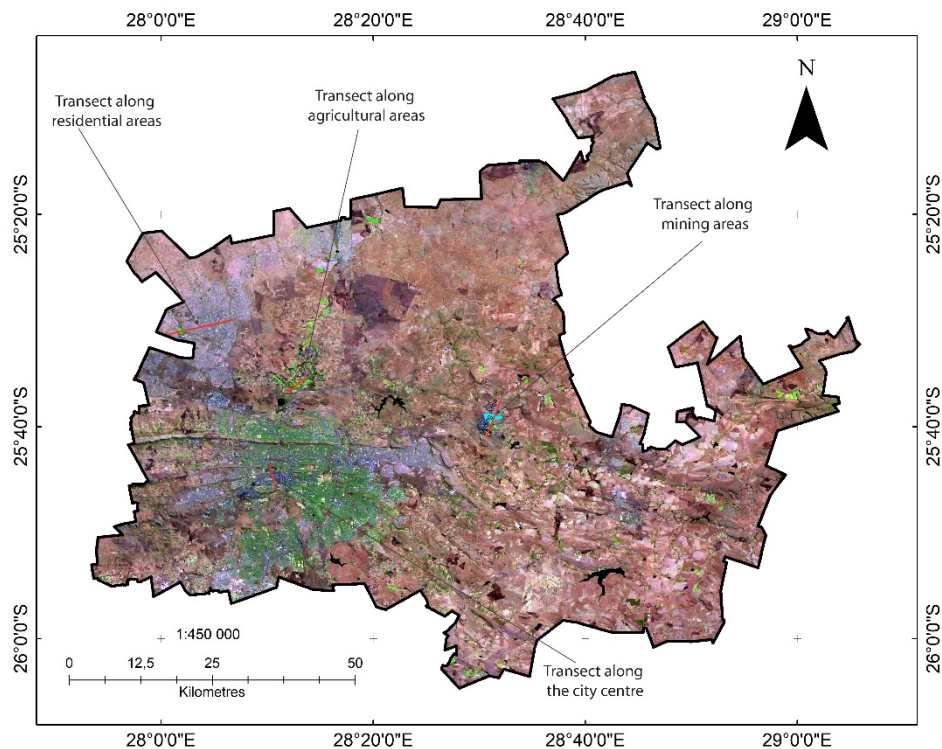
Figure 3: The location of transects that were used to assess LST variations along different land uses in the City of Tshwane.

4. Results and Discussions

4.1. Land Surface Temperature (LST)

Computed LST maps are depicted in Figure 4Higher temperatures were experienced in summer than in winter as depicted on the maps and there was an increase in temperature between 1997 and 2015. There was a higher LST in December 2015 compared to December 1997 and there were higher temperatures in summer compared to winter (Figure 5). The average temperature for December 2015 was 35.01°C, August 2015 was 30.44°C, December 1997 was 31.24°C and August 1997 was 20.95°C (Figure 5). Land surface temperature in urban areas was higher compared to the surrounding areas for August and December for both years. The results are in accordance with the consensus that there was higher LST in urban areas compared to the surrounding areas. This agrees with the finding from cities such as Cairo in Egypt, where there is little or no vegetation in urban areas (El-Magd *et al.*, 2016). CoT is also known as the Jacaranda City a pseudonym that was derived from the Jacaranda trees in the streets together with other different indigenous and alien tree species. These together with stadiums and parks in the urban areas plays a role on the LST in urban areas. The temperature in the city centre was lower than in urban environments outside the city. The high-density areas had higher temperatures compared to low-density areas and the city centres. This is mainly because there was less vegetation in high-density areas compared to low-density areas and the city centre.
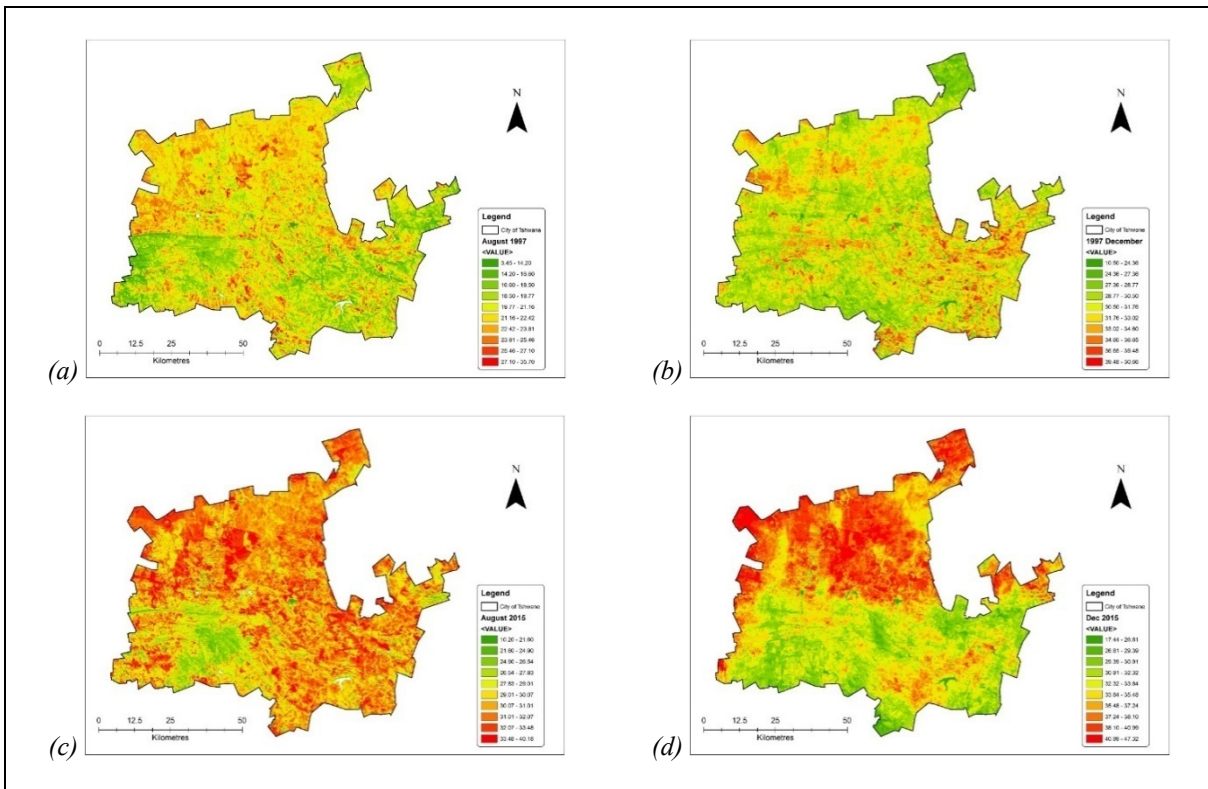
Figure 4: LST maps derived from the Landsat thermal bands and emissivity, a: August 1997, b: December 1997, c: August 2015 and d: December 2015
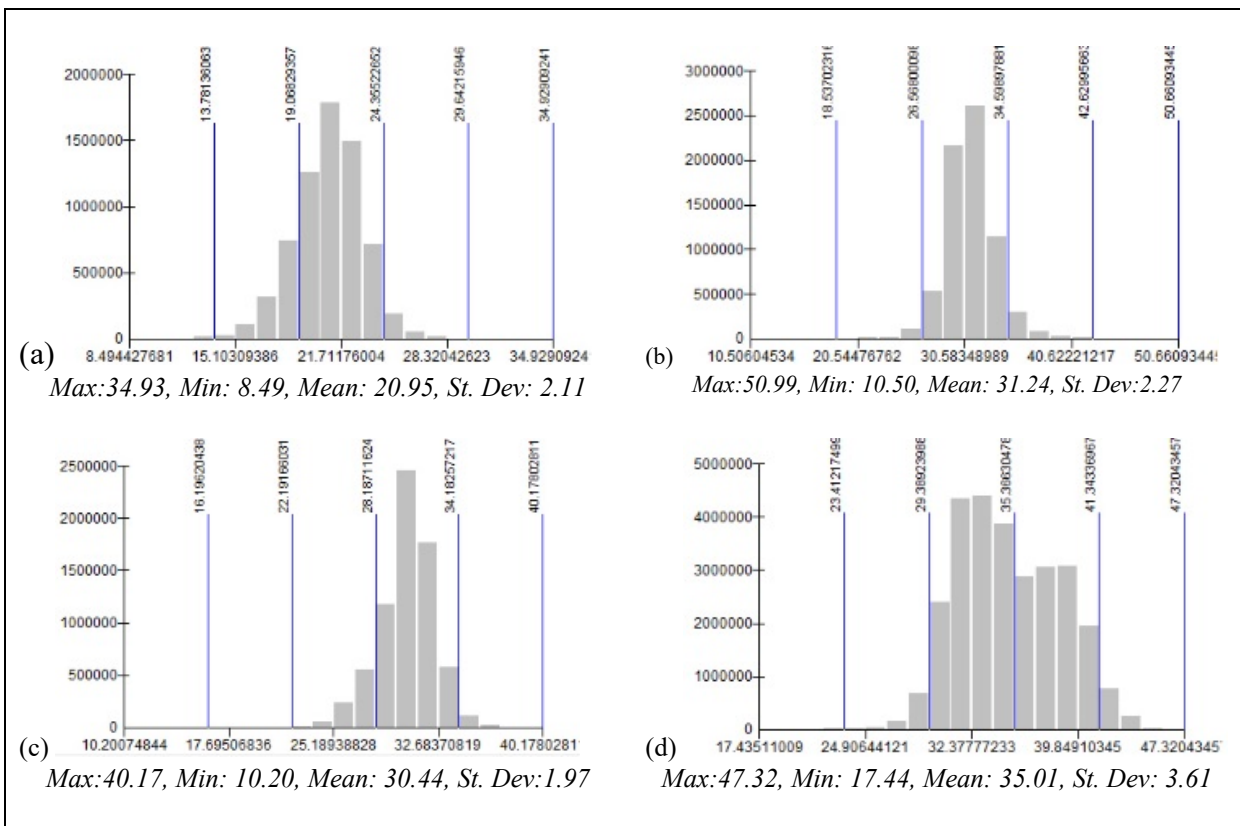

(a) Max:34.93, Min: 8.49, Mean: 20.95, St. Dev: 2.11

(b) Max:50.99, Min: 10.50, Mean: 31.24, St. Dev:2.27

(c) Max:40.17, Min: 10.20, Mean: 30.44, St. Dev:1.97

(d) Max:47.32, Min: 17.44, Mean: 35.01, St. Dev: 3.61

Figure 5: Statistics derived from the LST Maps of the City of Tshwane for the following months a: August 1997, b: December 1997, c: August 2015 and d: December 2015.

4.2. Normalised Land Surface Temperature

In August 1997, the normalised LST for August 1997 (Figure 6 (a)) had a mean of 0.47 with the standard deviation of 0.08 (Figure 7 (a)). Most of the areas were in the normal zone and green islands zone (0.2-0.4) and few heat islands. In December 1997, the normalised LST (Figure 6 (b)) had a mean of 0.51 and standard deviation of 0.06 (Figure 7 (a)). Most of the areas were in the normal zone and heat zone and fewer patches in strong heat islands (in red) (Figure 6 (b)). In August 2015, the normalised LST (Figure 6 (c)) had a mean of 0.68 and standard deviation of 0.07 (Figure 7 (c)). The normalised LST maps show most on the areas in the normal zone and fewer patches in the heat zone. In December 2015, the normalised LST (Figure 6 (d)) had a mean of 0.58 and standard deviation of 0.12 (Figure 7 (d)). There were significant strong heat islands zones in December 2015 but most of the areas were in the normal heat zones.
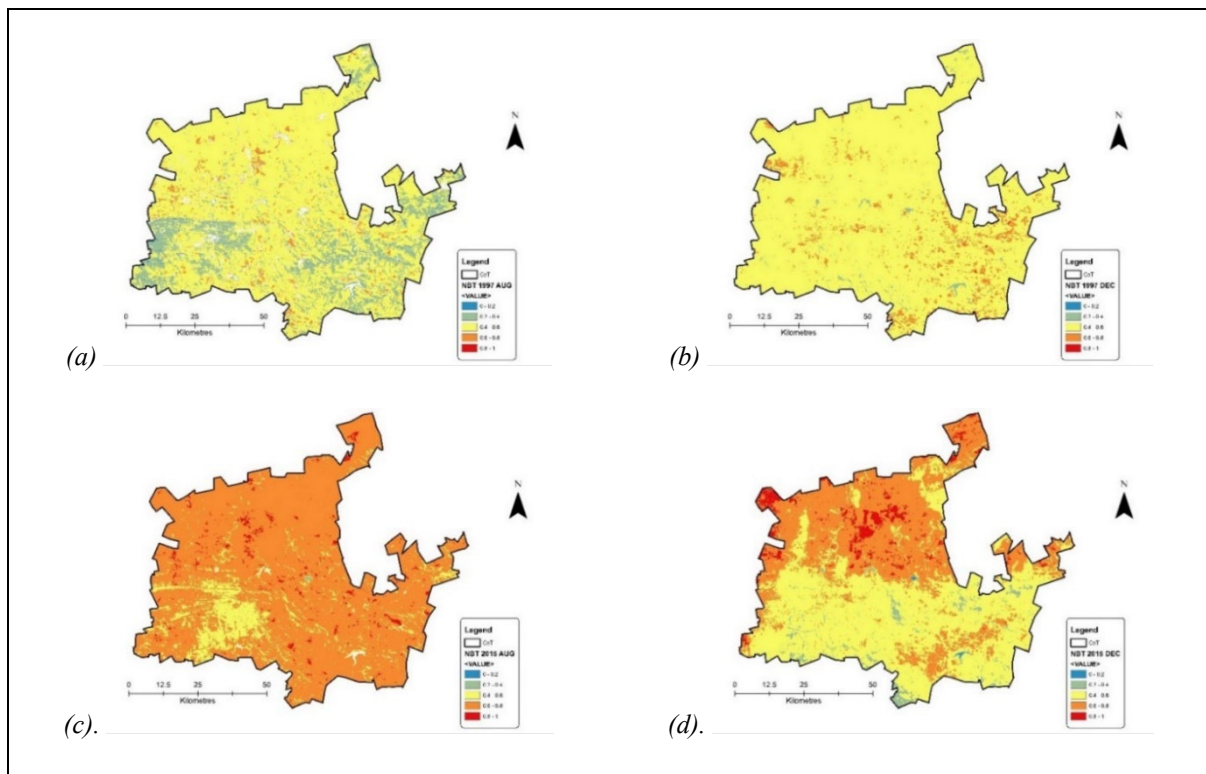

Figure 6: Normalised LST Maps derived from the LST Maps for a: August 1997, b: December 1997, c: August 2015 and d: December 2015.

(a)
Max:1,Min: 0,Mean: 0.47, St. Dev: 0.08

(b)
Max:1, Min: 0, Mean: 0.51, St. Dev:0.06

(c)
Max:1, Min: 0, Mean: 0.68, St. Dev:0.07
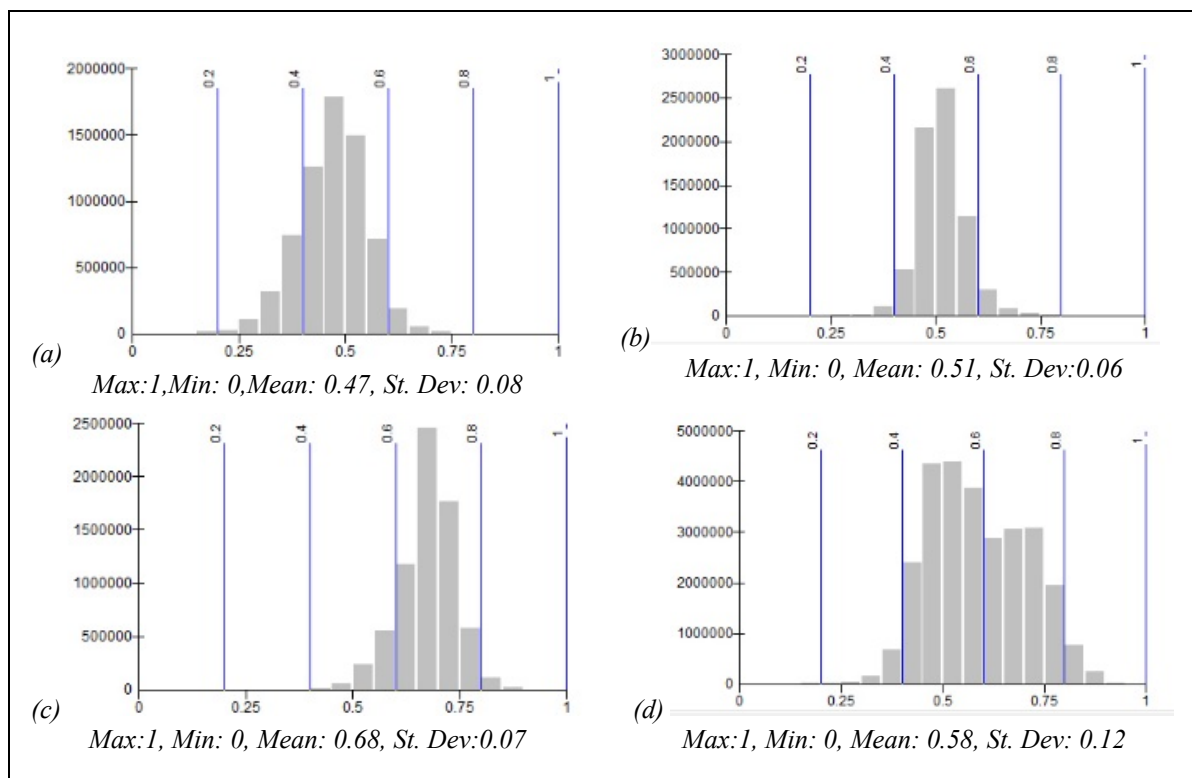
(d)
Max:1, Min: 0, Mean: 0.58, St. Dev: 0.12

Figure 7: Statistics derived from the Normalised LST Map of the City of Tshwane for a: August 1997, b: December 1997, c: August 2015 and d: December 2015.

4.3.   Spatial profile in Agricultural Areas

Spatial profiles of LST that were created along a transect in the agricultural areas are depicted in Figure 8. The spatial profiles revealed the inter-seasonal variations of LST 1997 and 2015 respectively. In the winter of 1997, the highest LST was 26.5°C, the lowest was 18.0°C and in summer of 1997, the highest temperature was 33.8°C with the lowest of 28°C. In the winter of 2015, the highest temperature was 33.2°C and lowest, was 23.5°C while in summer highest LST was 40.9 °C and lowest, was 29.3°C. There were peaks and depressions in the spatial profiles in both winter and summer images of 1997 and 2015. Peaks (high LST) were in areas with little or no crops and depressions (low LST) were in cropped areas where the value of greenness was high. Areas with depressions in winter were as a result of winter cropping and the winter cold weathers. There was a strong seasonality difference between the winter and summer seasons and it was clear in the spatial profiles of both 1997 and 2015. There was an increase in LST in agricultural areas between 1997 and 2015 in both seasons.
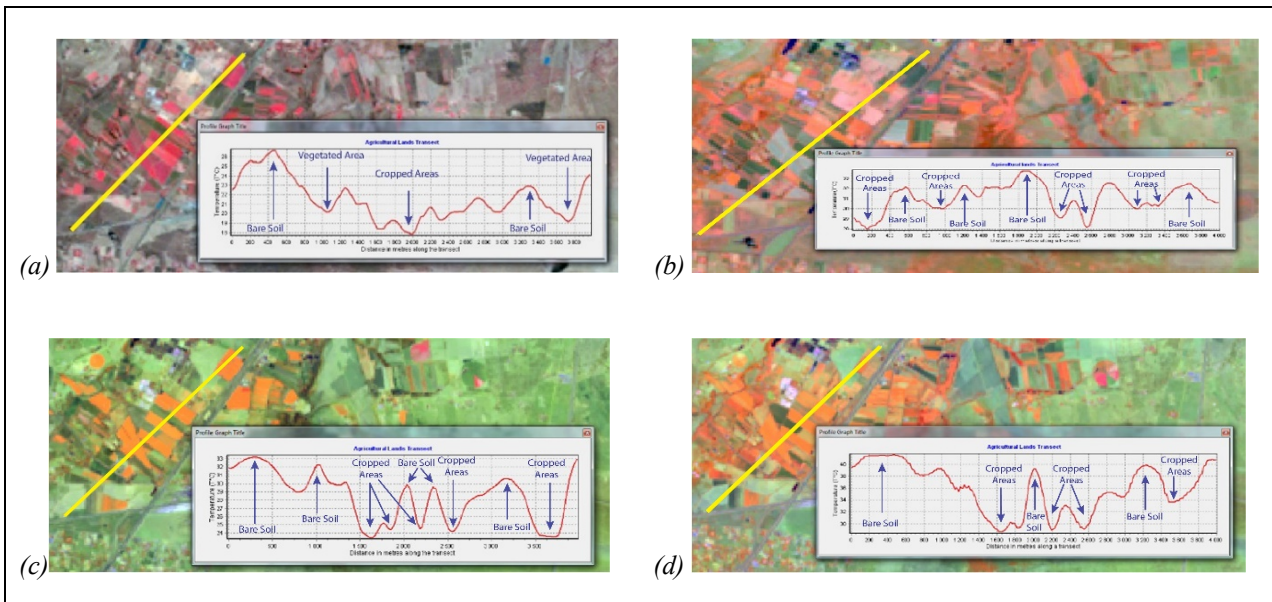
Figure 8: Spatial profile of LST along a transect (yellow) in the agricultural areas for a: August 1997, b: December 1997, c: August 2015 and d: December 2015.

4.4.   Spatial Profile in Residential Areas

The residential areas used in the study were in Soshanguve and the inter-seasonal variations for 1997 and 2015 are shown in Figure 9. In 1997 winter, highest temperature was 26.1°C and lowest, was 15.2°C while in summer highest LST was 36.5°C and lowest, was 23.1°C. In 2015 winter, highest LST was 33.6°C and lowest, was 23.2°C while in summer highest LST was 43.1°C and lowest, was 32.8°C. High peaks were experienced in newly established settlements where there was no vegetation and depression in areas with little or no impervious surface for example the water body which situated at 1500m from the start of the transect.
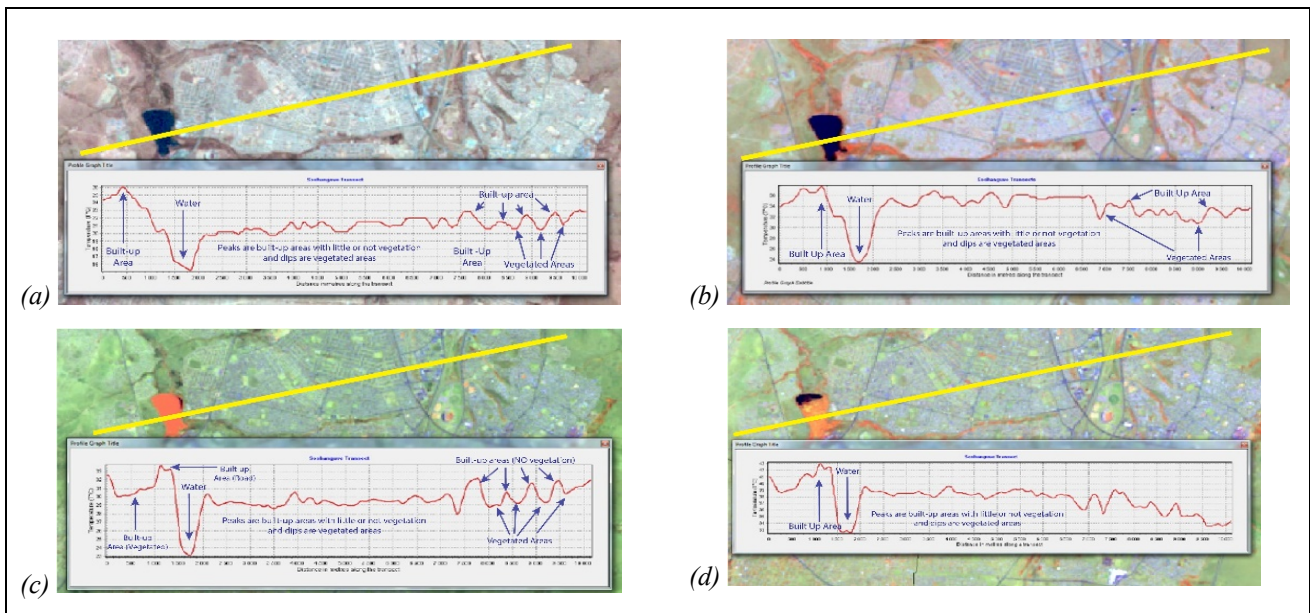

Figure 9: Spatial profile of LST along a transect (yellow) in the high-density residential areas of Soshanguve for a: August 1997, b: December 1997, c: August 2015 and d: December 2015.

4.5.   Spatial Profile in the City Centre

There were LST variations in the City Centre as shown Figure 10. In the winter of 1997, the highest LST was 21.0°C and lowest, was 15.1°C while in summer highest LST was 38.2°C and the lowest, was 27.8°C. In 2015 winter, the highest LST was 30.0°C and the lowest LST was 20.8°C while in summer the highest LST was 36.3°C and the lowest, was 29.8°C. Low LST in urban areas was a result of vegetation growth within the city and peaks were areas where there was no or little vegetation (bare soils and urban areas).
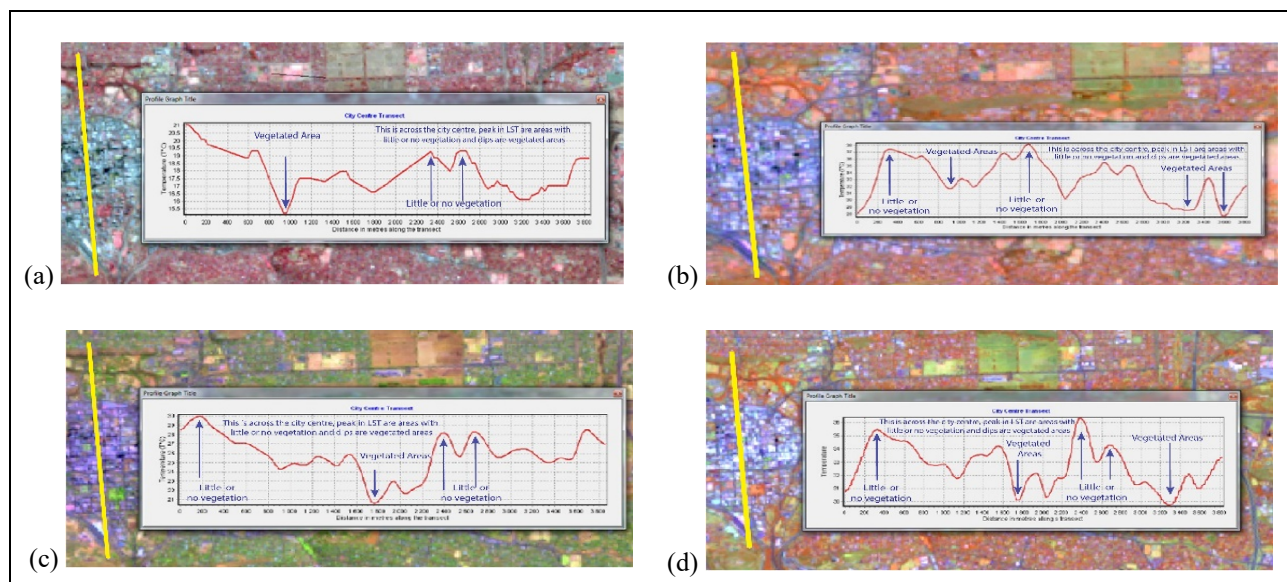

Figure 10: Spatial profile of LST along a transect (white) in the City Centre for a: August 1997, b: December 1997, c: August 2015 and d: December 2015.

4.6.   Spatial Profile in Mining Areas outside the City

There were LST variations in the mining area of Cullinan as shown Figure 11for the LST spatial profiles of 1997 and 2015 respectively. In winter of 1997, the highest LST was 25.0°C and the lowest, was 13.0°C while in summer, the highest LST was 34.8°C and the lowest, was 23.6°C. In winter of 2015, the highest LST was 34.5°C and the lowest LST was 17.5°C while in summer, the highest LST was 38.7°C and the lowest, was 22.0°C. There were some peaks and big depressions (dips) in LST, which was because of the opencast diamond mine, which is full of water. Some of the peaks were because of impervious surfaces and surrounding bare soils in the surrounding agricultural land. The depressions were due to vegetated and cropped areas in and around the Cullinan mine.
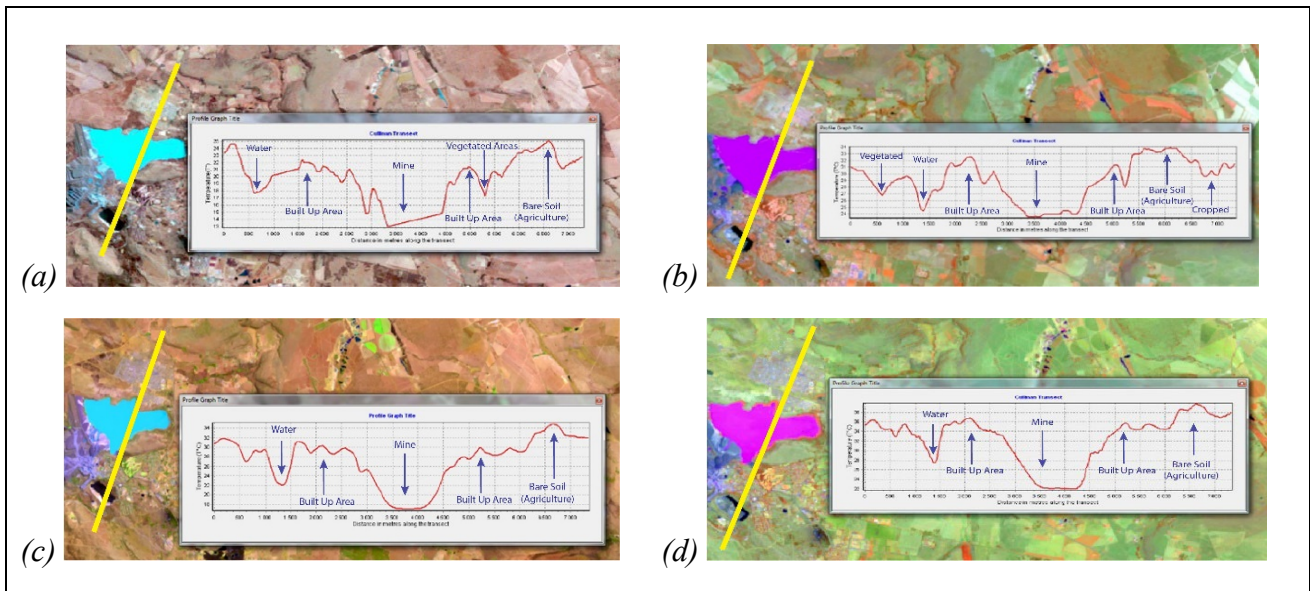
Figure 11: Spatial profile of LST along a transect (white) in mining area of Cullinan for a: August 1997, b: December 1997, c: August 2015 and d: December 2015.

4.7.   Relationship between NDVI and LST

The correlation coefficient between LST and NDVI was -0.5701728 and the p-value was 2.2e-16. These statistical values are quite significant, and they are in full agreement with outcomes from other researches (Abutaleb *et al.*, 2014; Adeline *et al.*, 2014; A Ngie *et al.*, 2016).
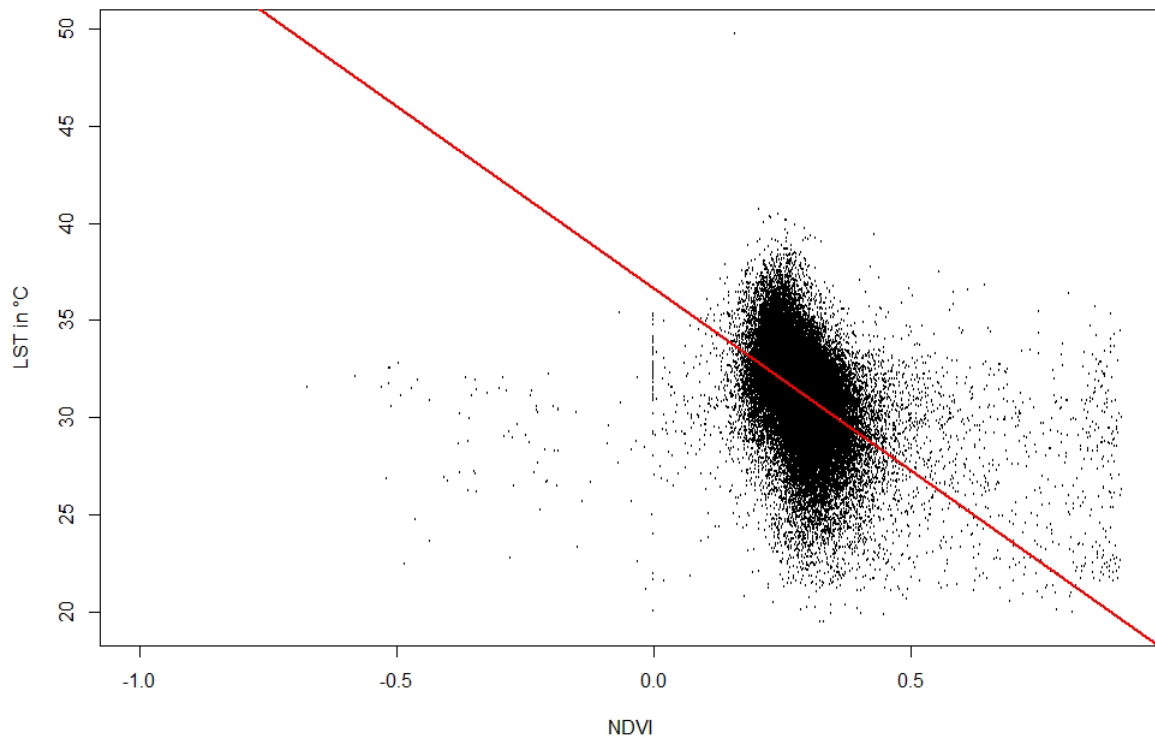

Figure 12: The scatterplot of LST against NDVI derived from the LST and NDVI bands using R programming and the regression line is in red.

4.8. Change in LST retrieved from MODIS (MOD11)

Variations in LST from 2000 and 2015 are as portrayed on Figure 13, retrieved from MOD11 remotely sensed data using Google Earth Engine. There is a progressive increase in LST in the CoT as shown on the trend line with an R^2 of 0.0015 and a gradient of 0.0001 and it showing a positive increase in LST. LST increases is as a result of the increase in impervious surfaces, signifying that urban areas are leading to the establishment of urban heat islands (Huidong Li *et al.*, 2018). LST increase in urban areas is attributed to the concentration of impervious surfaces and increase in air pollution, is also in agreement with the temperature data on Figure 14, which was acquired from the South African Weather Services where the trend line is showing a slightly increasing trend.
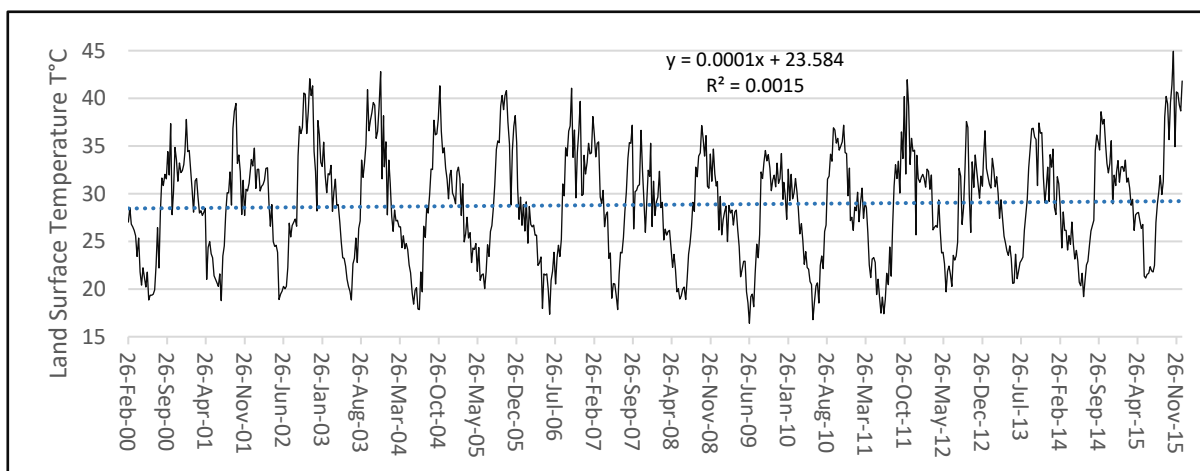

Figure 13: The temporal variation of LST derived from MODIS LST data using Google Earth Engine.
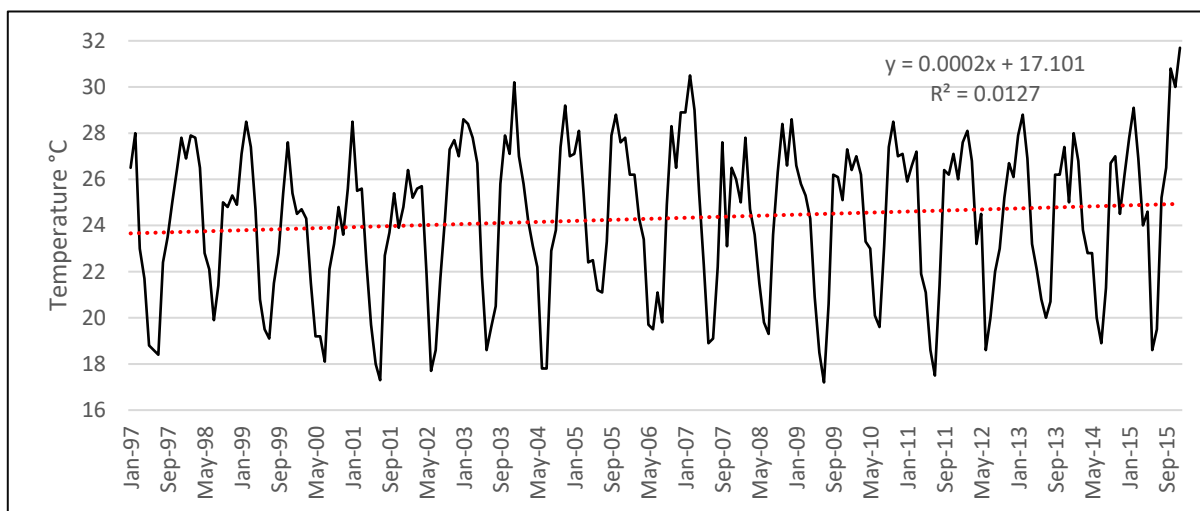

Figure 14: Variation in temperature in South Africa derived from meteorological stations.

Thermal profiles were used in this study to graphically illustrate spatial variations of LST in the urban environment and its surroundings and it showed curves of LST variations with cliffs, peaks, depressions and plateaus, which reveals the thermal variations in different land cover classes (Abebe, 2013; Abutaleb *et al.*, 2014; Huang *et al.*, 2008; Ngie *et al.*, 2014). Anthropogenic activities caused

transformation of natural to impervious surfaces, which affected the albedo, thermal capacity, heat conductivity (Ngie *et al.*, 2014). Adeyeri *et al.* (2017) argued that bare surfaces and built-up areas have high LST and low LST experienced in vegetated areas. This was in agreement with the results of this research. This argument was also supported by. In their study of Beijing China, there was a negative correlation between the amount of vegetation and urban heat islands. Bare surfaces experience high LSTs because of incident radiation, which was completely absorbed hence high LSTs (Adeyeri *et al.*, 2017; Ma *et al.*, 2008). Yue *et al.* (2007). Research done in Shanghai, China also revealed a negative correlation between NDVI and LST in the study, which indicated that where there was relatively low NDVI and little vegetation in the urban areas, there was high LST (Yue *et al.*, 2007). That was also supported in a study done in Kalaburagi, India by D. Kumar and Shekhar (2015). A significant increase in LST and spatial extent of urban heat islands were realised in many cities including Shanghai, China (J.-j. Li *et al.*, 2009).

Vegetation assists in reducing the LST of the environment and it also regulates the concentration of carbon in the atmosphere thereby reducing urban heat islands (Ali and Mohammed, 2016; Hui Li *et al.*, 2013). Vegetation provides shade, which reduces incident radiation and evapotranspiration, which helps to regulate overheating (Adeyeri *et al.*, 2017; Hui Li *et al.*, 2013; Mathew *et al*, 2017). Results of this study agree with research outputs by Adeyeri *et al.* (2017) which show that the lowest LST was in water bodies. Water is a special case in the mapping LST because it has low NDVI and low land surface temperature (D. Kumar and Shekhar, 2015). An urban area with green vegetation suffers less from LST than a non-vegetated urban area (Tomlinson *et al.*, 2012) and this was the case in the City Centre where low LST is being experienced due to increase in vegetation. There was a variation between winter and summer LST profile and an increase in LST from 1997 to 2015 in both seasons. In winter, there was low LST as compared to summer hence there was a significant difference in LST between the images of August (winter) and December (summer). In August, LST was lower compared to December in both 1997 and 2015. There was a significant increase in LST between 1997 and 2015 in both seasons and this can be attributed to climate change.

5. Conclusions

This study used remote sensing data to quantify and monitor LST and found that the thermal changes and urban heat island exist in the CoT. The urban thermal environment of CoT is an environmental issue leading to a need for a smart city planning with a focus on strategies for reduction in temperature that create comfortable living conditions within the area. It had been seen from the satellite-derived LST that the factors such as less percentage of green area and high built-up density are responsible for urban heating. The vegetated areas regulate the temperatures anomalies between the core city and the outskirts. The temperature is comparatively lower on the surroundings of the city than the centre. On the other hand, some peripheral areas, however, show a high-temperature and this can be due to the developments that would have taken place in the peripheral areas of the city and destruction of vegetation in this region. Water bodies and vegetation show very weak urban heat

island intensity, which implies that the availability of these land covers is essential for mitigating the thermal effects. The peripheral areas are also vulnerable to heating intensity, due to lack of vegetative cover and increasing barren land. Although the population density is very less in these areas, heat mitigation is the priority in these areas. The findings of this study could be helpful to the planners, land administrators, and decision-makers for adopting relevant and useful land use plans, e.g. green city plan, for mitigating the rising temperature and thermal discomfort of the city.

6. Acknowledgement

7. Reference

Abebe, G. A. (2013). Quantifying Urban growth pattern in developing Countries Using Remote Sensing and Spatial Metrics: A case study of Kampala, Uganda. *Msc Thesis*

Abutaleb, K., Adeline, N., Ahmed, F., Ahmed, M., Elkafrawy, S., Arafat, S., & Darwish, A. (2014). Investigation of Urban Heat Island Using Landsat Data. *Proceedings of the 10th International Conference of AARSE*, p 223.

Adeyeri, O. E., Akinsanola, A. A., & Ishola, K. A. (2017). Investigating surface urban heat island characteristics over Abuja, Nigeria: Relationship between land surface temperature and multiple vegetation indices. *Remote Sensing Applications: Society and Environment, 7*, pp. 57-68.
doi:http://dx.doi.org/10.1016/j.rsase.2017.06.005 Retrieved from
http://www.sciencedirect.com/science/article/pii/S2352938517300381

Ali, A., & Mohammed, E. (2016). Impact of Industrial Activities on Land Surface Temperature Using Remote Sensing and GIS Techniques-A Case Study in Jubail, Saudi Arabia. *J Geogr Nat Disast S, 6*, pp. 2167-0587.

Artis, D. A., & Carnahan, W. H. (1982). Survey of emissivity variability in thermography of urban areas. *Remote sensing of Environment, 12*(4), pp. 313-329. doi:http://dx.doi.org/10.1016/0034-4257(82)90043-8 Retrieved from http://www.sciencedirect.com/science/article/pii/0034425782900438

Chander, G., & Markham, B. (2003). Revised Landsat-5 TM radiometric calibration procedures and postcalibration dynamic ranges. *IEEE Transactions on geoscience and remote sensing, 41*(11), pp. 2674-2677.

El-Magd, I. A., Ismail, A., & Zanaty, N. (2016). Spatial Variability of Urban Heat Islands in Cairo City, Egypt using Time Series of Landsat Satellite Images. *International Journal of Advanced Remote Sensing and GIS*, pp. pp. 1618-1638.

ESRI. (2015). ArcGIS Desktop: Release 10. *Environmental Systems Research Institute*(Redlands, CA)

Harris, I., Jones, P. D., Osborn, T. J., & Lister, D. H. (2014). Updated high-resolution grids of monthly climatic observations–the CRU TS3. 10 Dataset. *International Journal of Climatology, 34*(3), pp. 623-642.

Huang, L., Li, J., Zhao, D., & Zhu, J. (2008). A fieldwork study on the diurnal changes of urban microclimate in four types of ground cover and urban heat island of Nanjing, China. *Building and environment, 43*(1), pp. 7-17.

Kumar, D., & Shekhar, S. (2015). Statistical analysis of land surface temperature–vegetation indexes relationship through thermal remote sensing. *Ecotoxicology and Environmental Safety, 121*, pp. 39-44.

doi:https://doi.org/10.1016/j.ecoenv.2015.07.004 Retrieved from
http://www.sciencedirect.com/science/article/pii/S0147651315300117

Kumar, K. S., Bhaskar, P. U., & Padmakumari, K. (2012). Estimation of land surface temperature to study urban heat island effect using LANDSAT ETM+ image. *International journal of Engineering Science and technology, 4*(2), pp. 771-778.

Laosuwan, T., Gomasathit, T., & Rotjanakusol, T. (2017). Application of Remote Sensing for Temperature Monitoring: The Technique for Land Surface Temperature Analyis. *Journal of Ecological Engineering, 18*(3), pp. 53-60.

Li, H., Harvey, J. T., Holland, T., & Kayhanian, M. (2013). The use of reflective and permeable pavements as a potential practice for heat island mitigation and stormwater management. *Environmental Research Letters, 8*(1), p 015023.

Li, H., Zhou, Y., Li, X., Meng, L., Wang, X., Wu, S., & Sodoudi, S. (2018). A new method to quantify surface urban heat island intensity. *Science of the total environment, 624*, pp. 262-272.

Li, J.-j., Wang, X.-r., Wang, X.-j., Ma, W.-c., & Zhang, H. (2009). Remote sensing evaluation of urban heat island and its spatial pattern of the Shanghai metropolitan area, China. *Ecological Complexity, 6*(4), pp. 413-420.

Ma, W., Chen, Y.-h., & Zhou, J. (2008). Quantitative analysis of land surface temperature-vegetation indexes relationship based on remote sensing. *Proc. 21st ISPRS Congress, Youth Forum*, pp. 261-264.

Magidi, J., & Ahmed, F. (2018). Assessing urban sprawl using remote sensing and landscape metrics: A case study of City of Tshwane, South Africa (1984–2015). *The Egyptian Journal of Remote Sensing and Space Science*

Mallick, J., Kant, Y., & Bharath, B. (2008). Estimation of land surface temperature over Delhi using Landsat-7 ETM+. *J. Ind. Geophys. Union, 12*(3), pp. 131-140.

Mathew, A., Khandelwal, S., & Kaul, N. (2017). Investigating spatial and seasonal variations of urban heat island effect over Jaipur city and its relationship with vegetation, urbanization and elevation parameters. *Sustainable Cities and Society, 35*, pp. 157-177. doi:http://dx.doi.org/10.1016/j.scs.2017.07.013 Retrieved from http://www.sciencedirect.com/science/article/pii/S2210670717304079

Mathew, A., Khandelwal, S., Kaul, N., & Chauhan, S. (2018). Analyzing the diurnal variations of land surface temperatures for surface urban heat island studies: Is time of observation of remote sensing data important? *Sustainable Cities and Society, 40*, pp. 194-213. doi:https://doi.org/10.1016/j.scs.2018.03.032 Retrieved from http://www.sciencedirect.com/science/article/pii/S2210670717310594

Matlala, R. L. (2015). *Institutional arrangements for the implementation of local economic development in Gauteng Province, with special reference to the City of Tshwane Metropolitan Municipality* (

Mucina, L., & Rutherford, M. (2006). The vegetation of South Africa, Lesotho and Swaziland. Strelitzia 19.,(South African National Biodiversity Institute: Pretoria, South Africa). *Memoirs of the Botanical Survey of South Africa*

Mushore, T. D., Odindi, J., Dube, T., Matongera, T. N., & Mutanga, O. (2017). Remote sensing applications in monitoring urban growth impacts on in-and-out door thermal conditions: A review. *Remote Sensing Applications: Society and Environment, 8*, pp. 83-93. doi:https://doi.org/10.1016/j.rsase.2017.08.001 Retrieved from http://www.sciencedirect.com/science/article/pii/S2352938517301167

Nega, W., Hailu, B. T., & Fetene, A. (2019). An assessment of the vegetation cover change impact on rainfall and land surface temperature using remote sensing in a subtropical climate, Ethiopia. *Remote Sensing Applications: Society and Environment, 16*, p 100266. doi:https://doi.org/10.1016/j.rsase.2019.100266 Retrieved from http://www.sciencedirect.com/science/article/pii/S2352938519301880

Neinavaz, E., Skidmore, A. K., & Darvishzadeh, R. (2020). Effects of prediction accuracy of the proportion of vegetation cover on land surface emissivity and temperature using the NDVI threshold method. *International Journal of Applied Earth Observation and Geoinformation, 85*, p 101984.

doi:https://doi.org/10.1016/j.jag.2019.101984 Retrieved from http://www.sciencedirect.com/science/article/pii/S030324341930618X

Ngie, A., Abutaleb, K., Ahmed, F., Darwish, A., & Ahmed, M. (2014). Assessment of urban heat island using satellite remotely sensed imagery: a review. *South African Geographical Journal, 96*(2), pp. 198-214.

Ngie, A., Abutaleb, K., Ahmed, F., Taiwo, O., Darwish, A., & Ahmed, M. (2016). An estimation of land surface temperatures from landsat ETM+ images for Durban, South Africa. *Rwanda Journal, 1*(1S).

Peres, L. d. F., Lucena, A. J. d., Rotunno Filho, O. C., & França, J. R. d. A. (2018). The urban heat island in Rio de Janeiro, Brazil, in the last 30 years using remote sensing data. *International Journal of Applied Earth Observation and Geoinformation, 64*, pp. 104-116. doi:https://doi.org/10.1016/j.jag.2017.08.012 Retrieved from http://www.sciencedirect.com/science/article/pii/S0303243417301770

Qin, Z., Karnieli, A., & Berliner, P. (2001). A mono-window algorithm for retrieving land surface temperature from Landsat TM data and its application to the Israel-Egypt border region. *International journal of remote sensing, 22*(18), pp. 3719-3746.

Schissau, R. (2006). Strafverfahren wegen MfS-Unrechts : die Strafprozesse bundesdeutscher Gerichte gegen ehemalige *Mitarbeiter des Ministeriums für Staatssicherheit der DDR*

Sheng, L., Tang, X., You, H., Gu, Q., & Hu, H. (2017). Comparison of the urban heat island intensity quantified by using air temperature and Landsat land surface temperature in Hangzhou, China. *Ecological Indicators, 72*(Supplement C), pp. 738-746. doi:https://doi.org/10.1016/j.ecolind.2016.09.009 Retrieved from http://www.sciencedirect.com/science/article/pii/S1470160X16305404

Sobrino, J. A., Jiménez-Muñoz, J. C., & Paolini, L. (2004). Land surface temperature retrieval from LANDSAT TM 5. *Remote sensing of Environment, 90*(4), pp. 434-440.

STATSSA, S. S. A. (2012). Census 2011 Municipal Report - Gauteng. [Report]. *Stats SA Library Cataloguing-in-Publication (CIP) Data*

Tomlinson, C., Chapman, L., Thornes, J., & Baker, C. (2012). Derivation of Birmingham's summer surface urban heat island from MODIS satellite images. *International Journal of Climatology, 32*(2), pp. 214-224.

Townshend, J. R., & Justice, C. (1986). Analysis of the dynamics of African vegetation using the normalized difference vegetation index. *International journal of remote sensing, 7*(11), pp. 1435-1445.

Weng, Q., Lu, D., & Schubring, J. (2004). Estimation of land surface temperature–vegetation abundance relationship for urban heat island studies. *Remote sensing of Environment, 89*(4), pp. 467-483.

Wray, C., & Cheruiyot, K. (2015). Key Challenges and Potential Urban Modelling Opportunities in South Africa, with Specific Reference to the Gauteng City-Region. *South African Journal of Geomatics, 4*(1), pp. 14-35.

Xu, L. Y., Xie, X. D., & Li, S. (2013). Correlation analysis of the urban heat island effect and the spatial and temporal distribution of atmospheric particulates using TM images in Beijing. *Environmental Pollution, 178*, pp. 102-114. doi:http://dx.doi.org/10.1016/j.envpol.2013.03.006 Retrieved from http://www.sciencedirect.com/science/article/pii/S026974911300122X

Yin, C. L., Meng, F., & Yu, Q. R. (2020). Calculation of land surface emissivity and retrieval of land surface temperature based on a spectral mixing model. *Infrared Physics & Technology, 108*, p 103333. doi:https://doi.org/10.1016/j.infrared.2020.103333 Retrieved from http://www.sciencedirect.com/science/article/pii/S1350449519311314

Yue, W., Xu, J., Tan, W., & Xu, L. (2007). The relationship between land surface temperature and NDVI with remote sensing: application to Shanghai Landsat 7 ETM+ data. *International journal of remote sensing, 28*(15), pp. 3205-3226.

Zhang, X. Q. (2016). The trends, promises and challenges of urbanisation in the world. *Habitat International, 54*(Part 3), pp. 241-252. doi:https://doi.org/10.1016/j.habitatint.2015.11.018 Retrieved from http://www.sciencedirect.com/science/article/pii/S0197397515302125